PROCEEDINGS OF SCIENCE

ONLINE ICRC 2021
THE ASTROPARTICLE PHYSICS CONFERENCE
Berlin | Germany
37th International Cosmic Ray Conference
12–23 July 2021

Validation of Monte Carlo Yield Function of a Semi-Leaded Neutron Monitor using Latitude Survey Data in 2019 and 2020

A. Seripienlert,[a,*] W. Nuntiyakul,[b] S. Khamphakdee,[b] P.-S. Mangeard,[c] A. Sáiz,[d] D. Ruffolo,[d] P. Evenson,[c] K. Fongsamut,[b] P. Jiang,[e] P. Chuanraksasat,[a] K. Munakata,[f] J. Madsen,[g] B. Soonthornthum[a] and S. Komonjinda[b]

[a] *National Astronomical Research Institute of Thailand (NARIT), Chiang Mai 50180, Thailand*
[b] *Department of Physics and Materials Science, Faculty of Science, Chiang Mai University, Chiang Mai 50200, Thailand*
[c] *Department of Physics and Astronomy, University of Delaware, Newark, DE 19716, USA*
[d] *Department of Physics, Faculty of Science, Mahidol University, Bangkok 10400, Thailand*
[e] *Polar Research Institute of China, Pudong, Shanghai 200136, China*
[f] *Physics Department, Shinshu University, Matsumoto, Nagano 390-8621, Japan*
[g] *Wisconsin IceCube Particle Astrophysics Center, University of Wisconsin-Madison, WI 53703, USA*
E-mail: achara@narit.or.th, waraporn.n@cmu.ac.th, sidarat_k@cmu.ac.th, mangeard@udel.edu, alejandro.sai@mahidol.ac.th, david.ruf@mahidol.ac.th, evenson@udel.edu, kanokkarn.f@gmail.com, jiangpeng@pric.org.cn, pongpichit.ch@gmail.com, kmuna00@shinshu-u.ac.jp, jim.madsen@icecube.wisc.edu, boonrucksar@narit.or.th, siramas.k@cmu.ac.th

A neutron monitor (NM) is a ground- (or sea-) based detector of the flux of cosmic ray particles in space. The high-energy cosmic rays in the GeV primary range interact in the upper atmosphere, producing a cascade of subatomic particles, some of which reach Earth's surface. A neutron monitor is mostly sensitive to the neutron component of the atmospheric cascade. These neutrons can then be detected by induced nuclear fission of ^{10}B in a $^{10}BF_3$ gas proportional counter. The Changvan neutron monitor is a portable neutron monitor assembled in Thailand and housed in a standard insulated shipping container to conduct long-term research in polar regions. There are three proportional counters housed in the insulated shipping container, but the central counter lacks the lead producer. We performed a Monte Carlo Simulation for the yield function of the Changvan monitor to primary particles. We validated our preliminary yield function by comparing count rates from simulation with actual data. We found that the maximum difference of the unleaded/leaded count rate ratio between simulation and experimental data was less than 7%. This leads to a promising yield function that can be used to determine the spectral index of relativistic solar ions with a single detector.

37th International Cosmic Ray Conference (ICRC 2021)
July 12th – 23rd, 2021
Online – Berlin, Germany

*Presenter

PoS(ICRC2021)1243

1. Introduction

Cosmic rays are high-energy charged particles from astrophysical sources. Cosmic rays can mostly be classified into two types according to their origin, solar energetic particles and Galactic cosmic rays (GCRs) from sources in our Galaxy outside the solar system. Primary cosmic rays are predominantly protons and alpha particles (99%), with about 1% heavier nuclei. When primary cosmic rays collide with atoms and molecules in the Earth's atmosphere, mainly oxygen and nitrogen, they produce a shower of lighter particles, e.g. neutrons, protons, and muons, known as secondary particles. Neutron monitors (NMs) are ground-based detectors that broadly used to detect secondary particles and monitor Galactic cosmic ray flux changes due to variations in the solar wind or solar storms. Hatton and Carmichael [1] designed the standard neutron monitor (NM64) containing boron trifluoride ($^{10}BF_3$)-gas proportional counters made at Chalk River Laboratories in Canada. The outermost polyethylene (PE) sheets of the NM64 are a reflector. When lower-energy particles from the environment collide with the PE reflector, they will be blocked. In contrast, the more energetic particles from the air shower can penetrate to the next component, lead rings. These lead rings are typically called the producer since they produce multiple lower-energy neutrons. We commonly call this production of several lower-energy neutrons from a single incident particle the "multiplicity." The next component inside the lead producer is a moderator made from high-density polyethylene to slow down the neutrons. The innermost component is a proportional counter filled with BF_3 gas, enriched to 96% of the ^{10}B isotope. The neutrons are detected by induced nuclear fission [^{10}B (n, α)^{7}Li]. The bursts of ionization eventually produce electrical pulses on a wire maintained at a potential of about -2,800 V. An electronic module counts these electric pulses and transmits them to the data-acquisition system.

In 2018, we built a mobile neutron monitor in Thailand to conduct a ship-borne latitude survey intending to detect secondary cosmic rays sweeping a wide range of geomagnetic cutoff rigidity (P_c). Geomagnetic cutoff rigidity i.e., the minimum rigidity required for charged particles to penetrate Earth's magnetic field, describes the shielding provided by Earth's magnetic field against the arrival of charged particles. The change in counting rate from a mobile monitor as a function of cutoff rigidity determines the Differential Response Function (DRF), which is the product of a yield function and the primary particle spectrum. The energy-dependent effective area (yield function) can be determined in two ways, direct-measurement latitude survey [2, 3] and Monte-Carlo simulation [4–7]. Each primary particle type has a yield function and a differential response function specific to a detector.

The count rate of a surface-mounted detector resulting from the impact of cosmic rays at the top of the atmosphere is the integral of the DRF function with rigidity ($P = pc/q$; momentum per charge). To simulate count rates for each counter tube in a mobile neutron monitor the yield function should be calculated, and the GCR spectrum, derived from the Local interstellar spectrum (LIS), which is assumed to be time invariant and a function of particle rigidity, must be calculated as a function of time. When lead-free and standard neutron monitors are operated in the same instrument, the different yield functions allow estimates to be made of the spectral indices for Ground Level Enhancement events [3]. There are two objectives for this work: (i) simulate the energy-dependent effective area (yield function, YF) for primary protons and alpha particles, and (ii) simulate the count rates of an individual tube and count rate ratios of unleaded/leaded as a

function of the geomagnetic cutoff rigidity. The comparison between the simulation results and the actual data from the latitude survey in 2019–2020 will be shown in this work.

2. Latitude Survey

2.1 Changvan neutron monitor

We built a mobile neutron monitor housed in a shipping container, nicknamed the "Changvan." We mounted the Changvan on the Chinese icebreaker *Xuelong* for two voyages between Shanghai, China, and Zhongshan station in Antarctica during 2019 and 2020 survey years. Figure 1 shows geometries of the semi-leaded 3NM64, shipping container, and *Xuelong* icebreaker. The Changvan neutron monitor contains three $^{10}BF_3$ proportional counters. The center counter lacks its own lead producer but has lead on either side, so we call this is a semi-leaded 3NM64. Three square plywood segments with holes in the center are used to hold the center counter at the correct spacing. The thickness of each plywood segment is 1.5 cm. The two outer counters include the ring-shaped lead producer, as in the standard design for the NM64.

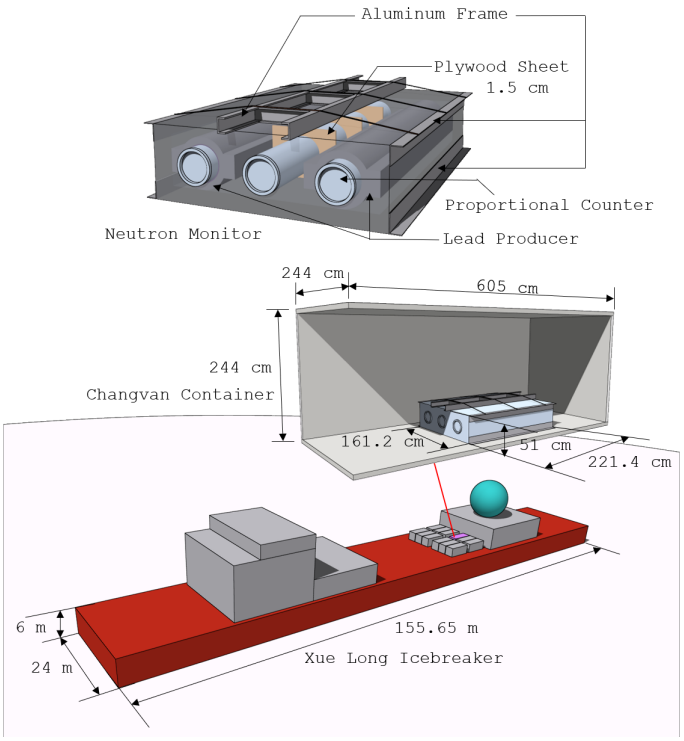

.

Figure 1: Changvan neutron monitor consists of 2 NM64s (with the lead producer) and an unleaded counter in the middle. Changvan was installed in an insulated shipping container and placed on the *Xuelong* icebreaker. This geometry is used in detector simulations. The renderings are created by Flair 3.1 [8]

2.2 Latitude Surveys during 2019–2020

During the 2019 and 2020 survey years, the Changvan was carried by the icebreaker *Xuelong* conducted by the Polar Research Institute of China (PRIC). The "survey year" refers to the year in

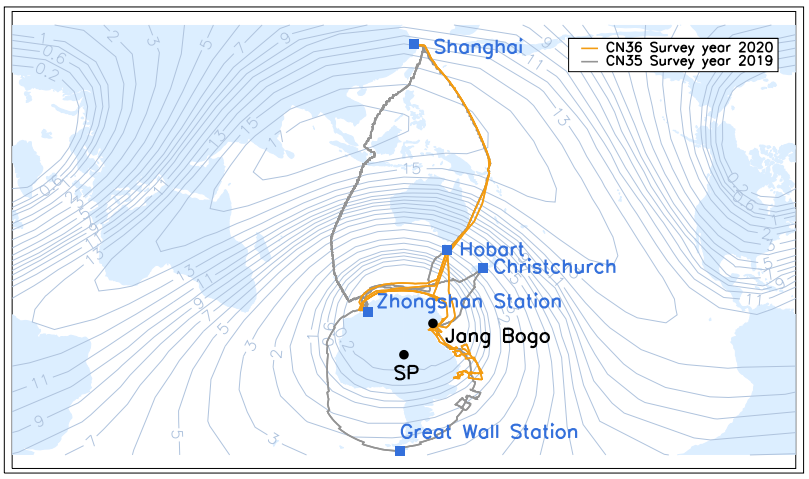

Figure 2: Path of Changvan neutron monitor in the 2019 (CN35: grey line) and 2020 (CN36: orange line) survey years. The contours with numbers indicate vertical cutoff rigidity (in the units of GV), calculated for February 11, 2019, at 12:00 UT.

which the voyage ended. The 2019 survey year covers the voyage from November 2, 2018 to March 11, 2019, and 2020 survey year covers the voyage from October 21, 2019 to April 22, 2020. The 2019 survey year is termed the 35th Chinese Antarctic Research Expedition (CN35), and the 2020 survey year is called CN36.

The geographic routes of the two surveys are plotted in Figure 2 where we also show contours of effective vertical geomagnetic cutoff rigidity (in units of GV), calculated for February 11, 2019, at 12:00 UT. Here we use the 12th Generation International Geomagnetic Reference Field (IGRF12), a standard mathematical description based on observed data of the Earth's main magnetic field integrated with a Tsyganenko model (semi-empirical best-fit representations based on satellite observations) for the magnetospheric field, to calculate the geomagnetic cutoff rigidity at the characteristic altitude of neutron production in the Earth's atmosphere. For the survey year 2019, the survey began on November 2, 2018, from Shanghai, China, at a cutoff rigidity of about 13.24 GV. There was an extensive port call in Hobart at approximately 1.24 GV, after which the survey continued to Zhongshan station, Antarctica. Note that in Earth's polar regions, the geomagnetic cutoff rigidity can be quite low, but the primary cosmic ray rigidity must exceed an atmospheric cutoff of approximately 1 GV for the atmospheric shower to generate counts in a ground-level neutron detector. The return trip was via Christchurch at about 2 GV, Antarctic Great Wall Station (the first Chinese research station), Zhongshan station again and then back to Shanghai on March 11, 2019. For the survey year 2020, the survey began on October 21, 2019, in Shanghai. Before reaching the Antarctic Zhongshan station the ship moored for some time in Hobart. The ship then left Zhongshan station to and from the Ross Sea, passing near the neutron monitor stations Jang Bogo and Mawson. The ship then headed straight back from Zhongshan station to Shanghai on April 22, 2020.

2.3 Data

Data were acquired with the standard acquisition system used in 13 surveys during 1994–2007 [9]. The counting rate of each detector was recorded once per second together with the attitude

of the ship (pitch and roll). Once per minute, the barometric pressure was recorded, as was the ship's position derived from GPS data. Apparent geomagnetic cutoffs [10–12] were calculated at one hour interval. We only have data for the second half of the 2019 survey year (from February 11 to March 11, 2019). Because of a heavy load of other shipping containers on CN35, we could not operate the Changvan on the voyage from Shanghai down to the Zhongshan station, a Chinese research station in Antarctica. In comparison, we have full data for the 2020 survey year (from October 21, 2019, to April 22, 2020). As we have more data in the subsequent survey year, we will only compare the simulation results with the results from that survey year. Here we used measured count rate vs. cutoff rigidity (P_c) from Yakum et al. (in preparation).

3. Monte Carlo Simulation

Our Monte Carlo simulations used FLUKA (FLUktuierende KAskade), version 4.1-1, which is an open-source particle physics package (https://fluka.cern/), [13, 14]. DPMJET hadron interaction models is using [15, 16]. The FLUKA simulation process used in this work can be divided into two parts: Atmospheric simulation and Detector simulation. Analysis of simulated yield function and count rates are done after completing the FLUKA simulation.

3.1 Atmospheric Simulation

We created an atmospheric profile using data from the Global Data Assimilation System (GDAS) and NRLMSISE-00, an empirical, global reference atmospheric model of the Earth from ground to space. We assumed a spherical atmosphere for the simulation, following the method described in [5] for the Hobart atmosphere in this work. We simulated isotropic primary particles with rigidity ranges from 1 GV to 200 GV; 1,000,000 events for each species of primary cosmic rays. These events produced secondary cosmic rays totaling 1,299,064 particles (136,508 neutrons, 13,486 protons, and 1,149,070 muons). These secondary cosmic rays are stored in libraries for use in the detector simulation in the next step.

3.2 Detector Simulation

Here, we use the detector geometry made with Flair 3.1 [8] shown in Figure 1. The geometry includes the Changvan monitor and structure surroundings provided by [17]. The container is placed on *Xuelong* icebreaker. We place seawater beneath the ship's entire lower half-spherical geometry. Secondary particles from the Libraries are chosen randomly and injected uniformly above the detector. We simulate 100,000,000 events for neutrons and protons and 75,000,000 events for muons. We applied deadtime 20 μs for all three tubes in the simulation. The results of the simulation are discussed in the next section.

4. Results and Conclusions

4.1 Yield Function of the Changvan monitor

From these simulations we calculated yield function of the Changvan neutron monitor for primary protons and alphas, shown in Figure 3 We observe the crossover between alpha and proton

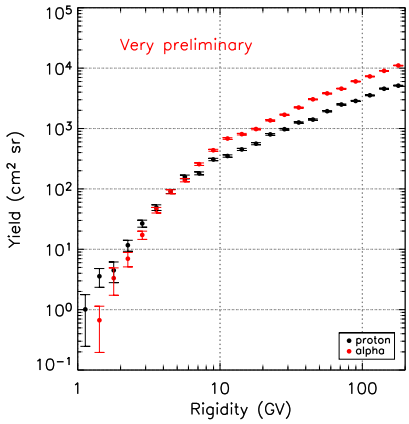

Figure 3: Yield functions for protons and alphas of Changvan neutron monitor.

yield functions at ~3-4 GV. At high rigidity, the yield function for alphas is higher than that for protons by a factor of ~2, roughly corresponding to the ratio of the total kinetic energy of an alpha and a proton at the same rigidity. The preliminary yields for alpha and proton seem reasonable, but we still need to do more simulations at lower rigidity than 6 GV for better statistics.

4.2 Count Rates vs. Cutoff Rigidity

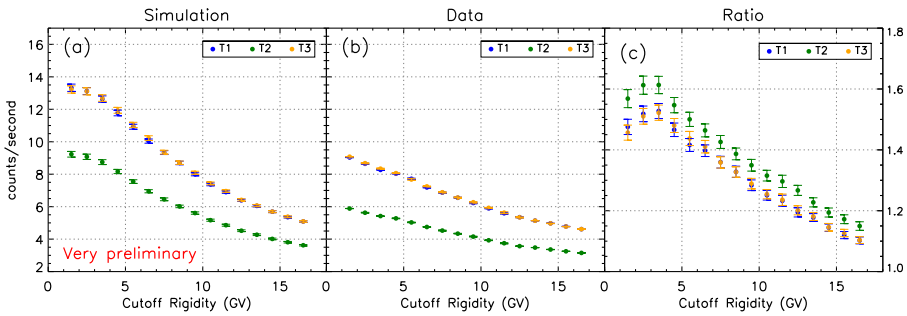

Figure 4: Comparison between (a) Simulation count rate and (b) Data count rate. The simulation count rate is higher than the Data count rate. The ratio of Simulation/Data count rate is provided in (c). The vertical error bar in (a)–(b) represents the standard error, and (c) the error propagation of the ratio; in many cases, the error bar is smaller than the plot symbol.

We estimated the primary GCR spectrum above the atmosphere from the Local Interstellar spectrum (LIS), corresponding to [19] with a solar modulation ϕ = 426 MV, as calculated from [18] to obtain count rates from simulations for individual tubes, shown in Figure 4. Here, T2 is the unleaded detector at the center, while T1 and T3 are leaded detectors flanking either side of the middle tube. Both simulation and data were corrected to a mean sea level pressure at P_0 = 760 mmHg using $C_p = Ce^{\beta(P-P_0)}$, where P is pressure, C is the count rate, and C_p is the count rate corrected for pressure variation. The barometric pressure coefficient β, in units of percent per mmHg, was empirically determined by [9] and depends on the cutoff rigidity P_c (in GV) as following $\beta = 1.006 - 0.01534P_c$ %/mmHg. Figure 4 (a) shows simulated count rates corrected for pressure, and Figure 4 (b) shows measured count rates corrected for pressure. Figure

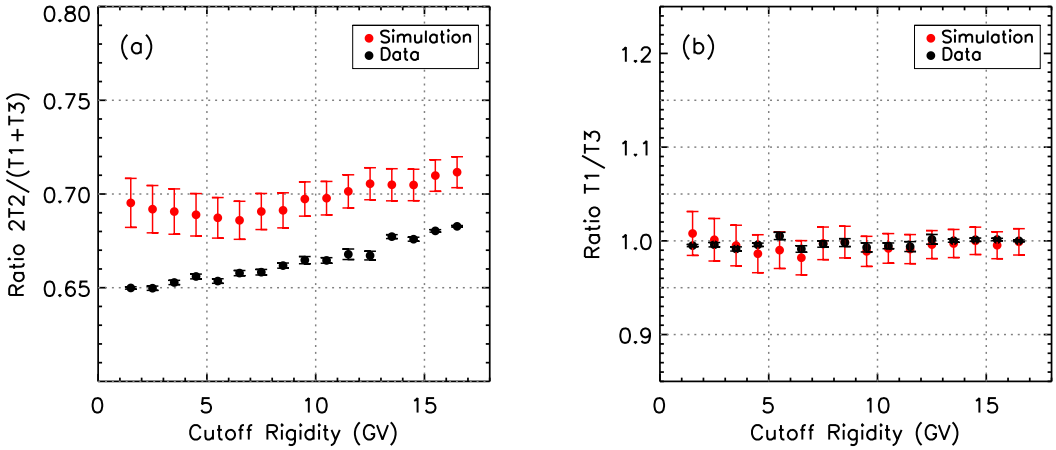

Figure 5: (a) The ratios of unleaded/leaded NM count rates. (b) The ratio of leaded/leaded NM rates. The vertical error bar represent the error propagation of the ratio, which still large for the simulated results.

4 (c) shows the ratio of the Simulation/Data count rate. We can see that the simulated count rates are overestimated for all rigidity bin (scale on the right shows numbers greater than 1).

4.3 Unleaded/Leaded Count Rate Ratios vs. Cutoff Rigidity

Such a Changvan semi-leaded 3NM64 can use the unleaded/leaded count rate ratio to determine the spectral index of relativistic solar ions with a single detector. Comparing simulation results for the ratio 2T2/(T1+T3) vs. cutoff rigidity to the actual ratio obtained from the latitude survey in Figure 5(a), we see that the simulated ratio was significantly higher than the actual count ratio across all cutoff rigidity ranges from 1-17 GV. The ratio T1/T3 vs. cutoff rigidity is near unity, as shown in Figure 5(b).

We can clearly see that the ratio of the actual count rate depends on the cutoff rigidity with a nearly linear trend, we also see a similar trend in the simulation result after 6 GV. Here, the obtained result is based on the Hobart atmosphere only. While conducting the actual experiment, the ship traveled through different atmospheres. In future work, we plan to modify some of the surrounding structures that affect the center unleaded tube more than the leaded tube and change the atmospheres corresponding to the actual observations. There is a very good agreement between the simulated and actual count rate ratio T1/T3. The size of the uncertainty propagation indicates that we need to do significantly more simulations to get statistically better results.

When we have a good result in Figure 4, it will lead us to obtain the comparable DRF to the actual result, and more precise yields for protons and alphas for further determination of the GCR spectrum.

5. Acknowledgments

This work was supported by NARIT, Chiang Mai University (CMU) and Thailand Science Research and Innovation via Research Team Promotion Grant RTA6280002. We thank ITC team of

NARIT and ITSC of CMU for providing server on-demand for simulations. We thank the Northern Science Park (Chiang Mai) for providing laboratory space at the park, which helps the research team working smoothly.

References

[1] Hatton, C.J. & H. Carmichael (1964), Can. J. Phys., 42, 2443–2472

[2] Nuntiyakul, W., Mangeard, P.-S., Ruffolo, D. et al (2020), J. Geophys. Res. Space Phys., 125, e27304

[3] Bieber, J. W., & Evenson, P. (1991), In Proc. of the 22nd ICRC, 3, 129–132

[4] Caballero-Lopez, R.A., & Moraal, H. (2012), J. Geophys. Res., 117, A12103

[5] Mangeard, P.-S., Ruffolo, D., Sáiz, A. et al (2016), J. Geophys. Res. Space Phys., 121, 7435–7448

[6] Mangeard, P.-S., Ruffolo, D., Sáiz, A. et al (2016), J. Geophys. Res. Space Phys., 121, 11,620–11,636

[7] Banglieng, C., et al. (2020), Astrophys. J., 890, 21

[8] V. Vlachoudis, "FLAIR: A Powerful But User Friendly Graphical Interface For FLUKA", in Proc. Int. Conf. on Mathematics, Computational Methods & Reactor Physics (M&C 2009), Saratoga Springs, New York, 2009.

[9] Nuntiyakul, W., P. Evenson, D. Ruffolo et al (2014), Astrophys J., 795, 11

[10] Lin, Z., J.W. Bieber, P. Evenson et al (1995), J. Geophys. Res., 100, 23,543–23,550

[11] Bieber, J.W. & J. Clem (1997), In Proc. of the 25th ICRC, 2, 389–392

[12] Clem, J., J. W. Bieber, P. Evenson (1997), J. Geophys. Res., 102, 26,919–26,926

[13] G. Battistoni, T. Boehlen, F. Cerutti et al. (2015), Ann. Nucl. Energy, 82, 10-18.

[14] T.T. Bohlen, F. Cerutti, M.P.W. Chin et al. (2014), Nucl. Data Sheets, 120, 211-214.

[15] S. Roesler, R. Engel, J. Ranft et al. (2001), Springer-Verlag Berlin, 1033-1038.

[16] A. Fedynitch, PhD Thesis, https://cds.cern.ch/record/2231593/files/CERN-THESIS-2015-371.pdf

[17] Fongsamut K., P., Jiang, W., Nuntiyakul et al. (2021), J. Phys Conf. Ser., 1719, 012004

[18] Usoskin I.G., A., Gil, G.A., Kovaltsov et al. (2017), J. Geophys. Res. Space Phys., 122, 3875–3887

[19] Vos, E.E. & M. S. Potgieter (2015), Astrophys. J., 815, 119